Investigating oil solubilization into nonionic micelles by Raman multivariate curve resolution

Ciera M. Wentworth[1#], Ryan L. Myers[1#], Paul S. Cremer[1,2*], Lauren D. Zarzar[1,3,4*]

1. Department of Chemistry, The Pennsylvania State University, University Park, PA 16802, USA
2. Department of Biochemistry and Molecular Biology, The Pennsylvania State University, University Park, PA, USA
3. Department of Materials Science and Engineering, The Pennsylvania State University, University Park, PA 16802, USA
4. Materials Research Institute, The Pennsylvania State University, University Park, PA 16802, USA

[#]These authors contributed equally to this work.
*Corresponding authors ldz4@psu.edu , psc11@psu.edu

Key words: Raman multivariate curve resolution, solubilization, micelle, hydrophobic hydration

Abstract

Hydrophobic hydration, whereby water spontaneously structures around hydrophobic and amphiphilic molecules plays a key role in hydrophobic interactions which are fundamental to the process of surfactant micelle formation and micellar oil solubilization. We characterized changes in the hydrophobic hydration of empty and oil-filled nonionic akylphenol ethoxylate surfactant Tergitol NP-12 micelles by vibrational Raman multivariate curve resolution (MCR) spectroscopy. We report trends in the changes of hydrophobic hydration depending on the chain length of the oil as well as the presence of a halogen atom in the structure. We find changes in hydrophobic hydration directly correlate to changes in micelle structure and physical properties of the micellar solution. We compare hydrophobic hydration trends of Tergitol NP-12 to nonionic linear alkyl ethoxylate surfactant Makon TD-12 and ionic sodium dodecyl sulfate and observe similar trends. Interestingly, we find the oil itself has the largest impact on the hydrophobic hydration, micelle structure, and physical properties. We believe these studies contribute to a fundamental understanding of the importance of hydrophobic hydration in surfactant and oil aggregates, especially as it relates to micellar oil solubilization, and provide insight into how the molecular solubilizate can impact micellar structure, size, and stability.

Introduction

Surfactants are amphiphilic molecules that stabilize interfaces by lowering the interfacial tension (γ) between two phases. For water-soluble surfactants above the critical micelle concentration (CMC), surfactant monomers aggregate into nanometer-sized structures called micelles due to the hydrophobic effect[1,2]. For micelles formed in water, the micelle contains a hydrophilic exterior and a hydrophobic interior core into which hydrophobic molecules can be partitioned. Surfactants and micelles are thus widely used in research and application for cleaning[3,4], dispersing[5,6], mixing[7–9], and chemical separations[10–12]. Hydrophobic hydration is a

phenomenon in which hydrophobic or amphiphilic molecules induce spontaneous structuring of water[13,14]. Hydrophobic hydration is theorized to play a fundamental role in hydrophobic interactions, which are vital to micellar oil solubilization[15–18]. Yet, there is gap in our knowledge about the hydrophobic hydration of nonionic micelles compared to the hydrophobic hydration of ionic micelles, whose charge effects between headgroups dominate their solvation and dynamics in solution[14,19]. Here, using the emerging technique of vibrational Raman multivariate curve resolution (MCR) spectroscopy, we investigate the impact of oil solubilization on the hydrophobic hydration and structure of nonionic surfactant micelles in water.

Nonionic surfactants are those in which the headgroup is polar and uncharged. These amphiphilic molecules tend to be physiologically mild and are not prone to precipitating or denaturing proteins and nucleic acids, and thus are widely used in pharmaceuticals, cosmetics, and industrial formulations. Furthermore, surfactants with polyethylene oxide (PEO) hydrophilic headgroups are chemically compatible with most water-soluble organic and inorganic compounds and remain effective over a wide range of pHs values, rendering them suitable for a wide variety of uses[20]. Due to the lack of headgroup charge, it has been suggested that solubilizates (e.g. oils) can be present not only in the hydrophobic core of the micelle, but at the hydrophilic-hydrophobic boundry[21,22], as well as within the PEO palisade[23,24], depending on the structure of the nonionic surfactant. In addition, most commercial nonionic surfactants are polydisperse, leading some authors to find, such as in the case of Triton X-100, that the micelles have overlapping internal and external surfactant molecules, leading to an ill-defined hydrophilic-hydrophobic boundary generating more difficulty in identifying solubilization sites[25]. 2D NOESY has shown that when heptane is solubilized into Triton X-100 micelles, it disrupts the layered micelle structure and the formation of cross peaks were observed. These cross peaks indicate that the oil interacts with the PEO headgroup and the heptane dehydrates the surfactant molecules[24]. Contrastingly, Goldenberg *et al*.[26] find not all solubilizates can solubilize into the PEO palisade and can be confined to the core. These results highlight that solubilization is the product of a complex interaction between the surfactant and solubilizate and cannot be strictly predicted by the surfactant hydrophilic PEO and hydrophobic lengths. Where the relationship is not only governed by the surfactants structural features, but is also determined properties of the solubilizate including its polarity, polarizability, lipophilicity, chain length and branching, which can also influence the degree of solubilization and distribution within the micelle. And that many experimental techniques and methods such as quasi light scattering, 2D NOESY NMR, UV, ^{13}C NMR, and solvent model systems all have limitations in determining solubilizate location and micellar strucutre[26].

Raman multivariate curve resolution (MCR) spectroscopy is an emerging vibrational spectroscopy technique capable of identifying solute-induced perturbations of solvent molecules. When a solute is added to a solvent, typically, only the first hydration shell around the solute is affected, thereby leaving the vast majority of the solvent molecules undisturbed. Thus, when conducting vibrational spectroscopy, signal from the unperturbed solvent in the bulk tends to dominate and hides changes in the hydration layer. A home-built Raman setup was used to obtain a 1000:1 signal to noise in order to use MCR analysis to deduce hydration information. Raman MCR has thus been employed to study the hydrophobic hydration and structure of ions[27–29], small hydrophobic molecules[30–32], polymers[33,34] and surfactant micelles[35,36]. Since the hydrophobic effect drives the aggregation of surfactant molecules, measuring changes in the

hydrophobic hydration of micelles can provide fundamental information regarding micelle structure and properties[14]. Thus far, use of Raman MCR has been limited to studying the hydrophobic hydration of ionic surfactants and micelles, such as decyltrimethylammonium bromide and sodium octanoate[35,36]. For example, Long et. al. [35] observed dangling OH peak features with ionic sodium decanoate micelle formation, suggesting that water can penetrate into the hydrophobic tail region of a micelle, hydrating up to 20% of the surfactant methylene groups; the size of these hydrated cavities also depended upon the chain length of the surfactant. Researchers also observed that when sodium decanoate and decyltrimethylammonium bromide ionic micelles are swollen with d-hexane, the oil resides in the dry oil-like core of the micelle[35]. However, one might hypothesize that the water structure within nonionic surfactant micelles with PEO headgroups may be fundamentally different than the water structure in an ionic surfactant micelle due to the nature of the electrostatic and solvation interactions[37]. By characterizing the solvated water around nonionic micelles, we can gain insight into hydrophobic interactions and changes within the micelle with oil solubilization, thus providing solubilizate distribution and solubilization efficacy.

Here we characterize the hydrophobic hydration changes of nonylphenol ethoxylate Tergitol NP-12 micelles by systematically solubilizing oils of varying lengths and halogenation (n-alkanes, n-bromoalkanes, and n-iodoalkanes). We explore trends in oil length, halogenation, as well as oil orientation and solubilization sites. We find hydrophobic hydration is highly influenced by oil length, where shorter chain oils displace the most water from the micelle while longer chain oils displace a minimal amount of water from the micelle. Oil halogenation only contributes to large changes in hydrophobic hydration with shorter oil chain lengths and becomes less relevant as the chain length is extended. We compare these results to a linear alkyl ethoxylate nonionic surfactant Makon TD-12 and an ionic surfactant sodium dodecyl sulfate (SDS) and observe similar trends in hydrophobic hydration, making the solubilized oil the most significant factor in predicting hydrophobic hydration changes. Our results suggest hydrophobic hydration changes of micellar solutions that undergo oil solubilization directly impact the micellar structure and the physical properties of the micelle.

Results and Discussion

We first aimed to develop a Raman MCR procedure to characterize the perturbed water in and around a nonionic micelle composed of an alkylphenol ethoxylate, Tergitol NP-12. To begin, we examined the MCR spectrum of 1 wt% Tergitol NP-12 in H_2O but found extensive overlap was present between the water OH stretch from 2800-3800 cm^{-1} and the surfactant CH stretches at approximately 2700-3100 cm^{-1}. Since we needed to define a baseline using the surfactant's aromatic CH centered at ~3080 cm^{-1}, this overlap made consistently defining the baseline difficult. To avoid aromatic CH/ OH stretch peak overlap, we switched D_2O as the solvent. Deuterating the water causes the OH stretch to red shift from ~3300 cm^{-1} to ~2400 cm^{-1} (OD stretch) thereby allowing for more consistent baseline determination and greater signal resolution from the CH stretches. We next wanted to determine if the contribution from the dissolved surfactant monomer (as compared to the micelles) had a significant effect on the Raman signal, so we took a spectrum of 0.005 wt% Tergitol NP-12, which is below the surfactant CMC of 0.0085 wt%; we found that the OH intensity of 0.005 wt% NP-12 was near zero (**Figure S1**). We concluded that the surfactant monomer had no observable effect on the Raman signal,

and thus any signal we measure for surfactant concentrations above the CMC is dominated by micelles. To obtain an optimal signal to noise ratio, we collected the spectra of 1, 3, and 5 wt% Tergitol NP-12 and found that 5 wt% Tergitol NP-12 yielded a strong, reproducible signal (**Figure 1a**). We thus used 5 wt% Tergitol NP-12 for most of the following experiments.

We next aimed to determine if there was an observable difference between a Raman spectrum of the empty (unsaturated) 5 wt% Tergitol NP-12 micelles and that of the oil-filled (saturated) 5 wt% Tergitol NP-12 micelles (**Figure 1a-b**). We collected a background spectrum of pure D_2O, which represents unperturbed bulk solvent (i.e. light-blue "Bulk D_2O" in **Figure 1b-i**). We then took a Raman spectrum of empty 5 wt% Tergitol NP-12 micelles which includes signal from the micelles, bulk D_2O, and the D_2O that is perturbed by solvating the micelles (i.e. the dark blue inside the dotted line of the "empty micelle" in **Figure 1b-i**). We next collected the Raman spectrum of 5 wt% Tergitol NP-12 with hexane solubilized into the micelle, which contains signal from the micelle, bulk D_2O, perturbed water, and oil (**Figure 1b-i**). (For the oil solubilization procedure refer to experimental methods in the SI). The MCR algorithm was used to deconvolute the signal from the surfactant and surfactant-perturbed water from the bulk water in the region 2200-2700 cm^{-1} (**Figure 1b-ii**). This allowed us to isolate changes in the micellar-solvated D_2O when transitioning from empty to oil filled micelles (comparing the dark blue water encompassed within the dotted lines of **Figure 1b-i**). The signal contribution from the oil in the CH region of the spectrum is expected to be minimal, since the oil is present in mM or lower concentrations, which is significantly less than the surfactant. **Figure 1b-ii** shows the MCR spectra of unsaturated 5 wt% Tergitol NP-12 versus hexane-saturated 5 wt% Tergitol NP-12, where we see a ~25% decrease in perturbed water when hexane is added to the micelle. This decrease indicates that when hexane is solubilized into the micelle, some of the water that previously had solvated the micelle was removed.

Having developed a protocol to investigate the hydrophobic hydration of the nonionic micelles, we then probed the impact of the solubilized alkane oil length and halogenation on the micelle hydration. We saturated 5 wt% NP-12 micelles with hexane, octane, decane, and hexadecane. We expected significant differences in hydrophobic hydration as previous cryo-TEM studies on Triton X-100 revealed alkane chain length directly impacts interactions between surfactant molecules and affects overall micelle aggregation[38]. As shown in the MCR graphs in **Figure 2a**, as the chain length of the alkane increases, less perturbed water is removed from the micelle. Solubilization of hexane removes the most water, contributing to an MCR area decrease of 25%. Solubilization of hexadecane expels the least amount of water with only an 11% MCR area decrease. We were interested in how small changes in polarizability of the oil, such as by addition of a halogen, might affect the dehydration of the PEO headgroups of the Tergitol NP-12 micelle and whether a halogenated oil might have an orientation dependence within the micelle. We used MCR to analyze the perturbed water for 5 wt% Tergitol NP-12 saturated with 1-bromoalkanes and 1-iodoalkanes with carbon numbers of 6, 8, 10, and 16. Within each halogenated oil series, (bromo and iodo) we observed similar trends as for the alkanes, where the amount of expelled water decreased with increasing carbon number (**Figure 2b**). As shown in **Figure 2b**, we found that, generally, that bromoalkanes and iodoalkanes contribute to larger MCR area decreases than alkanes, with approximately 20% more displaced water (i.e. less total perturbed water) from the micelles for oils with carbon numbers six and eight. However, for a carbon number of 16, halogenation (bromo or iodo), did not have a significant impact on the

dehydration of the micelle. Interestingly, we did not observe a significant difference in the change in hydrophobic hydration when comparing oil-filling of bromoalkanes and iodoalkanes. This was surprising because the iodo moiety is sufficiently large compared to the bromo moiety so one might suspect the iodoalkanes to expel more water from the micelle than bromoalkanes. But this is not what was observed and just having the halogen moiety on the oil contributed to more water being expelled from the micelle than the size of the halogen.

Due to the large differences in the amount of expelled water from the micelle between oil chain lengths six and sixteen, we hypothesized that short and long chain oils solubilize differently within the micelle, with the potential for multiple solubilization sites[21–24]. We observed changes in the ratio between pi-hydrogen bond (hydrogen on water pointing towards aromatic group, pi interaction) at 2703 cm^{-1}, and the free OH (hydrogen on water pointing towards a hydrophobic molecule) at 2732 cm^{-1}, see **Figure S2**. For shorter oil chain lengths, the pi-hydrogen (pi-H) interaction disappears, indicating that the oil is displacing the water that was surrounding the aromatic group on Tergitol NP-12. At longer oil chain lengths, the pi-H interaction is present at similar quantities as was observed for empty micelles. In **Figure 2c** we have plotted the pi-H to free OH intensity ratio of the various oils added to the NP-12 micelle. The low peak intensity ratio of pi-H to free OH shows that water interacting with the pi aromatic group decreases for shorter chain oils (ratio below 1.0). Oils with a chain length of sixteen have the highest peak intensity ratio of 1.4 (with oil-filling) with the unsaturated micelle having a ratio of 1.7. These results suggest that shorter oils, which are also more water-soluble and PEO-soluble, may be able to penetrate further outside of the hydrophobic core into the headgroup region of the NP-12 micelle, while longer oils, that tend to be less soluble in water and PEO, sit in the hydrophobic core of the micelle and do not penetrate into the PEO headgroups. To determine if the halogenated oils induced any structural changes to the micelle or possessed any preferential orientation within the NP-12 micelle, we performed high resolution (1800 gratings/mm) MCR on the CH stretch region (2700-3100 cm^{-1}) of the micelle for a series of iodoalkanes (**Figure 2d**). We found no change in the CH region, which signified that there was no significant change in the hydrophobic environment and observable structural modifications within the micelle or preferential oil orientation within the micelle.

We aimed to gain insight into how the hydrophobic hydration trends observed with Raman MCR correlate with physical properties of the Tergitol NP-12 micelles (e.g. micelle hydrodynamic diameter, solubilization capacity, and cloud points). We used dynamic light scattering (DLS) to determine how the micelle hydrodynamic diameter changes upon oil solubilization. As shown in **Figure 3a**, the hydrodynamic diameter of the NP-12 micelle is 9.0 $\pm$ 0.2 nm, and the hydrodynamic diameter increased significantly upon solubilization of oils with six to ten carbons. However, for oil with 16 carbons, we did not observe a significant size change within error (**Table S1** for all values). Varying the halogen atom of the oil had little impact on the micelle hydrodynamic diameters, which may be expected because the molar volume change with the different halogen is minimal. As expected, the cloud point shows little difference between brominated and iodinated oils, but there were large differences between oils of varying chain length, where decreasing the carbon number from sixteen to six yielding a significant reduction in the cloud point from 77.1 $\pm$ 0.2 ^{o}C to below 55 ^{o}C (**Figure 3b)**. The cloud point depression for shorter chain oils was expected due to the fact it has the largest impact on hydrophobic hydration

where the oil is effectively dehydrating the PEO headgroup and a similar effect has been observed in the literature with other surfactants[39,40].

The general observations regarding hydrodynamic diameter and cloud point trends mirrored the results for the changes in MCR area, where the longest chain length oils also had the least impact on the micelle structure and amount of perturbed water. We hypothesized that these trends might be related to the varying capacity of the micelles to solubilize oils of different chain lengths. We measured the approximate solubilization capacity of each oil in 5 wt% NP-12 (**Table S2**). Overall, we found solubilization capacity decreases as oil length increases, which is consistent with literature[41]. Oils with 6, 8, 10, and 16 carbons have a capacity of roughly 10 µL/mL, 8 µL/mL, 5 µL/mL, and less than 0.2 µL/mL, respectively. For each, we calculated approximately how many oil molecules there are per micelle, using an estimated aggregation number of 100 surfactant molecules per micelle, yielding approximately 100, 70, 30, and 1 oil molecule(s) per micelle respectively. We surmise that the higher solubilization capacity for shorter chain oils compared to that of longer chain oils may be due to the fact that the smaller oil can interact with the surfactant's PEO headgroup in addition to the hydrophobic tail, thus providing increased solubilization sites, and also leading to increases in the hydrodynamic diameter and decreasing the cloud point[42]. In contrast, longer chain oils are limited to solubilizing within the micelle hydrophobic core, which leads to a much reduced solubilization capacity and limited changes to the micelle structure and physical properties. In order to estimate the oil miscibility in the PEO palisade, we used a refractometer to extrapolate between the refractive indices of the pure bromoalkane and pure poly(ethylene glycol) (average molecular weight 200) (PEG 200) in order to obtain volume fractions that average to the measured refractive index (refer to experimental methods in SI). We find the degree of miscibility of the bromoalkanes in PEG 200 is significantly large compared to their water solubility, calculating 1.1 M, 0.80 M, 0.63 M, and 0.0 M for bromoalkanes with chain lengths 6, 8, 10, and 16 respectively. Thus, suggesting the oil's PEO solubility is an important factor in predicting solubilization capacity, solubilization sites, and significant changes in hydrophobic hydration with micellar oil solubilization.

Having extensively explored the properties of an alkylphenol ethoxylate surfactant Tergitol NP-12, we wanted to examine how changes in the surfactant chemical structure would alter the hydrophobic hydration and micellar solubilization capacity. We chose to examine an alkyl ethoxylate surfactant, Makon TD-12, which has the same PEO headgroup size distribution as the Tergitol NP-12 but has only a linear alkyl tail and no aromatic ring. We hypothesized that due to the absence of the aromatic group, we might observe a difference in the amount of perturbed water and impact of oil filling; however, as shown in **Figure 4a**, we observe similar MCR area decreases and trends to that observed for Tergitol NP-12 (**Figure 2b**). We also measured similar trends in the Makon TD-12 micelle hydrodynamic diameter with oil solubilization (**Table S1**). Interestingly, the measured solubilization capacity of 5 wt% Makon TD-12, was less than that of Tergitol NP-12, for oils of 6, 8, 10, and 16 carbons having a capacity of roughly 6.5 µL/mL, 5 µ/mL, 3 µL/mL, and less than 0.2 µL/mL, respectively, indicative of the fact that the tail of the nonionic surfactant is an important determinant in oil solubilization capacity (**Table S2**). We believe 5 wt% Makon TD-12 has a reduced solubilization capacity to 5 wt% Tergitol NP-12 even though there PEO headgroup is the same length because the CMC of Makon is higher at 0.013 wt%, thus fewer micelles are present in solution to effectively solubilize oil.

To contextualize our findings regarding the hydrophobic hydration and micelle structure nonionic surfactants, we wanted to compare the results for nonionic surfactants with that of an ionic surfactant, sodium dodecyl sulfate (SDS). SDS micelles have not been characterized by Raman MCR previously, although other ionic surfactant micelles such as sodium octanoate, sodium decanoate, and decyltrimethylammonium bromide have been studied[35,36]. As shown in **Figure 4b**, we contrast 5 wt% Tergitol NP-12, 5 wt% Makon TD-12, and 1 wt% SDS with solubilized n-iodoalkanes. We used 1 wt% SDS instead of 5 wt% SDS to obtain a clear and consistent baseline, as increasing the concentration caused baseline nonlinearity. When 1 wt% SDS micelles were saturated with 1-iodohexane, we observed an MCR area decrease of 35%, which was comparable to the results obtained for both the Tergitol NP-12 and Makon TD-12, meaning a similar amount of water was displaced for each surfactant upon oil saturation. However, for longer chain oils (8, 10, and 16), the SDS micelles had significantly less displaced water than the nonionic surfactants. Non-linear baselines in SDS due to impurities in the surfactant created difficulty in analyzing MCR data which lead to large errors in the MCR area percent decrease. It is not believed that the MCR area percent decrease for 1-iodohexadecane can be negative, which would suggest an increase in perturbed/solvated water around the oil-swollen micelle compared to the empty micelle but is instead attributed to challenges in the non-linear background of the spectrum. Interestingly, we also observed little change in the hydrodynamic diameter of the SDS micelle with oil filling (**Table S1**). Based on previous studies using Vibrational Sum Frequency Spectroscopy (VSFS), that characterize the effects of charges at the interface[37], these changes in hydrophobic hydration were expected. Where the strong charge interactions dominate the ordering of water beyond the first hydration shell, and the partitioning of the oil into the surfactant micelle leaves the ordering unaffected. Thus making the oil, the single most important factor in determining changes in hydrophobic hydration in ionic SDS micelles as well as nonionic Tergitol NP-12 and Makon TD-12 micelles.

Conclusions

We have explored the hydrophobic hydration dynamics of oil solubilization of nonionic surfactants Tergitol NP-12, Makon TD-12, and ionic surfactant SDS. Most prominently, we observed that short chain oils release the most water from the micelle and affect the overall structure and physical properties of the micelle. Longer chain oils displace little water from the micelle and do not have a significant effect on the micelles structure and physical properties. The disappearance of the pi-H peak for shorter chain oils suggested that shorter chain oils can solubilize to the micelle interior as well as the PEO palisade, while longer chain oils tend to only solubilize into the hydrophobic core and do not disrupt the water pi interaction. We also found that halogenation of the oil contributes to much larger changes in hydrophobic hydration at shorter oil lengths and does not contribute to signifcant changes in hydrophobic hydration at long chain lengths. Lastly, when Tergitol NP-12 was compared to Makon TD-12 and SDS, we observed similar trends in hydrophobic hydration changes with oil length, where shorter oils displace the most water from the micelle while longer oils displace the least. These findings indicate the oil has a direct impact on the micellar solubilization, stability, structure, and physical properties of the micelle. We hope these results provide insight onto how solubilizate structure can be manipulated to influence micellar structure and properties as solubilization vehicles for a wide use of technologies and applications.

***Acknowledgements*.**
C. W. and L. Z. acknowledge funding support from the Army Research Office (W911NF-18-1-0414) and the Packard Foundation (2019-69664). R.M. and P.C. acknowledge funding support from the National Science Foundation (CHE-2004050). The authors would also like to acknowledge Tinglu Yang for his expertise and construction of the home-built Raman experimental setup.

References

(1) Ben-Amotz, D.; Mendes De Oliveira, D. Surfactant Aggregate Size Distributions above and below the Critical Micelle Concentration. *J. Chem. Phys.* **2021**, *155* (22). https://doi.org/10.1063/5.0071246.
(2) Khoshnood, A.; Lukanov, B.; Firoozabadi, A. Temperature Effect on Micelle Formation: Molecular Thermodynamic Model Revisited. *Langmuir* **2016**, *32* (9), 2175–2183. https://doi.org/10.1021/acs.langmuir.6b00039.
(3) Cox, M. F. Surfactants for Hard-Surface Cleaning: Mechanisms of Solid Soil Removal. *J. Am. Oil Chem. Soc.* **1986**, *63* (4), 559–565. https://doi.org/10.1007/BF02645756.
(4) Scheibel, J. J. The Evolution of Anionic Surfactant Technology to Meet the Requirements of the Laundry Detergent Industry. *J. Surfactants Deterg.* **2004**, *7* (4), 319–328. https://doi.org/10.1007/s11743-004-0317-7.
(5) Zhu, Z.; Song, X.; Cao, Y.; Chen, B.; Lee, K.; Zhang, B. Recent Advancement in the Development of New Dispersants as Oil Spill Treating Agents. *Curr. Opin. Chem. Eng.* **2022**, *36*, 100770. https://doi.org/10.1016/j.coche.2021.100770.
(6) Prasanna Shankara, R.; Banapurmath, N. R.; Souza, A. D.; Dhaded, S. S. Experimental Investigation of Enhanced Cooling Performance with the Use of Hybrid Nanofluid for Automotive Application. *IOP Conf. Ser. Mater. Sci. Eng.* **2020**, *872* (1). https://doi.org/10.1088/1757-899X/872/1/012074.
(7) Harnby, N. Edwards, M. F. N. A. W. *Mixing in the Process Industries: Second Edition*, Second edi.; Butterworth-Heinemann, 1992.
(8) Fradette, L.; Brocart, B.; Tanguy, P. A. Comparison of Mixing Technologies for the Production of Concentrated Emulsions. *Chem. Eng. Res. Des.* **2007**, *85* (11 A), 1553–1560. https://doi.org/10.1205/cherd06015.
(9) James, A. Overview of Asphalt Emulsion. *Transp. Res. Circ.* **2006**, No. August, 1–15.
(10) Frankewich, R. P.; Hinze, W. L. Evaluation and Optimization of the Factors Affecting Nonionic Surfactant-Mediated Phase Separations. *Anal. Chem.* **1994**, *66* (7), 944–954. https://doi.org/10.1021/ac00079a005.
(11) Scamehorn, John Harwell, J. *Surfactant Based Separation Processes*; Marcel Dekker: New York, 1989.
(12) Hinze, Willie Pramauro, E. A Critical Review of Surfactant-Mediated Phase Separations (Cloud Point Extractions): Theory and Applications. *Crit. Rev. Anal. Chem.* **1993**, *24* (2), 133–177.
(13) Jiménez-Ángeles, F.; Firoozabadi, A. Hydrophobic Hydration and the Effect of NaCl Salt in the Adsorption of Hydrocarbons and Surfactants on Clathrate Hydrates. *ACS Cent. Sci.* **2018**, *4* (7), 820–831. https://doi.org/10.1021/acscentsci.8b00076.
(14) RomstedLaurence. Do Amphiphile Aggregate Morphologies and Interfacial Compositions

Depend Primarily on Interfacial Hydration and Ion-Specific Interactions? The Evidence from Chemical Trapping. *Langmuir* **2006**, *22* (22), 32–41.
(15) Patel, A. J.; Varilly, P.; Jamadagni, S. N.; Hagan, M. F.; Chandler, D.; Garde, S. Sitting at the Edge: How Biomolecules Use Hydrophobicity to Tune Their Interactions and Function. *J. Phys. Chem. B* **2012**, *116* (8), 2498–2503. https://doi.org/10.1021/jp2107523.
(16) Meister, K.; Strazdaite, S.; DeVries, A. L.; Lotze, S.; Olijve, L. L. C.; Voets, I. K.; Bakker, H. J. Observation of Ice-like Water Layers at an Aqueous Protein Surface. *Proc. Natl. Acad. Sci. U. S. A.* **2014**, *111* (50), 17732–17736. https://doi.org/10.1073/pnas.1414188111.
(17) Laage, D.; Elsaesser, T.; Hynes, J. T. Water Dynamics in the Hydration Shells of Biomolecules. *Chem. Rev.* **2017**, *117* (16), 10694–10725. https://doi.org/10.1021/acs.chemrev.6b00765.
(18) Ahmed, M.; Singh, A. K.; Mondal, J. A. Hydrogen-Bonding and Vibrational Coupling of Water in a Hydrophobic Hydration Shell as Observed by Raman-MCR and Isotopic Dilution Spectroscopy. *Phys. Chem. Chem. Phys.* **2016**, *18* (4), 2767–2775. https://doi.org/10.1039/c5cp07014g.
(19) Zdrali, E.; Chen, Y.; Okur, H. I.; Wilkins, D. M.; Roke, S. The Molecular Mechanism of Nanodroplet Stability. *ACS Nano* **2017**, *11* (12), 12111–12120. https://doi.org/10.1021/acsnano.7b05100.
(20) Schott, H. Krafft Points and Cloud Points of Polyoxyethylated Nonionic Surfactants: The Effect of Hydrotropes and Other Organic Electrolytes. *Tenside, surfactants, Deterg.* **2009**, *46* (1), 39–47.
(21) Gokhale, D.; Chen, I.; Doyle, P. S. Coarse-Grained Molecular Dynamics Simulations of Immobilized Micelle Systems and Their Interactions with Hydrophobic Molecules. *Soft Matter* **2022**, *18* (24), 4625–4637. https://doi.org/10.1039/d2sm00280a.
(22) Rangel-Yagui, C. O.; Hsu, H. W. L.; Pessoa, A.; Tavares, L. C. Micellar Solubilization of Ibuprofen - Influence of Surfactant Head Groups on the Extent of Solubilization. *Rev. Bras. Ciencias Farm. J. Pharm. Sci.* **2005**, *41* (2), 237–246. https://doi.org/10.1590/S1516-93322005000200012.
(23) Mukerjee, P. Solubilization of Benzoic Acid Derivatives by Nonionic Surfactants: Location of Solubilizates in Hydrocarbon Core of Micelles and Polyoxyethylene Mantle. *J. Pharm. Sci.* **1971**, *60* (10), 1528–1531. https://doi.org/10.1002/jps.2600601019.
(24) Giorgio, G.; Colafemmina, G.; Mavelli, F.; Murgia, S.; Palazzo, G. The Impact of Alkanes on the Structure of Triton X100 Micelles. *RSC Adv.* **2016**, *6* (1), 825–836. https://doi.org/10.1039/c5ra21691e.
(25) Denkova, P. S.; Lokeren, L. Van; Verbruggen, I.; Willem, R. Self-Aggregation and Supramolecular Structure Investigations of Triton X-100 and SDP2S by NOESY and Diffusion Ordered NMR Spectroscopy. *Society* **2008**, *112*, 10935–10941.
(26) Goldenberg, Merrill. Bruno, Lisa. Rennwantz, E. Determination of Solubilization Sites and Efficiency of Water-Insoluble Agents in Ethylene Oxide-Containing Nonionic Micelles.Pdf. *J. Colloid Interface Sci.* **1993**, No. 158, 351–363.
(27) De Oliveira, D. M.; Zukowski, S. R.; Palivec, V.; Hénin, J.; Martinez-Seara, H.; Ben-Amotz, D.; Jungwirth, P.; Duboué-Dijon, E. Binding of Divalent Cations to Acetate: Molecular Simulations Guided by Raman Spectroscopy. *Phys. Chem. Chem. Phys.* **2020**, *22* (41), 24014–24027. https://doi.org/10.1039/d0cp02987d.

(28) Ahmed, M.; Namboodiri, V.; Singh, A. K.; Mondal, J. A.; Sarkar, S. K. How Ions Affect the Structure of Water: A Combined Raman Spectroscopy and Multivariate Curve Resolution Study. *J. Phys. Chem. B* **2013**, *117* (51), 16479–16485. https://doi.org/10.1021/jp4100697.

(29) Drexler, C. I.; Miller, T. C.; Rogers, B. A.; Li, Y. C.; Daly, C. A.; Yang, T.; Corcelli, S. A.; Cremer, P. S. Counter Cations Affect Transport in Aqueous Hydroxide Solutions with Ion Specificity. *J. Am. Chem. Soc.* **2019**, *141* (17), 6930–6936. https://doi.org/10.1021/jacs.8b13458.

(30) Davis, J. G.; Gierszal, K. P.; Wang, P.; Ben-Amotz, D. Water Structural Transformation at Molecular Hydrophobic Interfaces. *Nature* **2012**, *491* (7425), 582–585. https://doi.org/10.1038/nature11570.

(31) Perera, P. N.; Fega, K. R.; Lawrence, C.; Sundstrom, E. J.; Tomlinson-Phillips, J.; Ben-Amotz, D. Observation of Water Dangling OH Bonds around Dissolved Nonpolar Groups. *Proc. Natl. Acad. Sci. U. S. A.* **2009**, *106* (30), 12230–12234. https://doi.org/10.1073/pnas.0903675106.

(32) Gierszal, K. P.; Davis, J. G.; Hands, M. D.; Wilcox, D. S.; Slipchenko, L. V.; Ben-Amotz, D. Π-Hydrogen Bonding in Liquid Water. *J. Phys. Chem. Lett.* **2011**, *2* (22), 2930–2933. https://doi.org/10.1021/jz201373e.

(33) Mochizuki, K.; Ben-Amotz, D. Hydration-Shell Transformation of Thermosensitive Aqueous Polymers. *J. Phys. Chem. Lett.* **2017**, *8* (7), 1360–1364. https://doi.org/10.1021/acs.jpclett.7b00363.

(34) Rogers, B. A.; Okur, H. I.; Yan, C.; Yang, T.; Heyda, J.; Cremer, P. S. Weakly Hydrated Anions Bind to Polymers but Not Monomers in Aqueous Solutions. *Nat. Chem.* **2022**, *14* (1), 40–45. https://doi.org/10.1038/s41557-021-00805-z.

(35) Long, J. A.; Rankin, B. M.; Ben-Amotz, D. Micelle Structure and Hydrophobic Hydration. *J. Am. Chem. Soc.* **2015**, *137* (33), 10809–10815. https://doi.org/10.1021/jacs.5b06655.

(36) Plastinin, I. V.; Dolenko, T. A. MCR-Raman Spectroscopy of Sodium Octanoate Micelles in Aqueous Solutions. *Vib. Spectrosc.* **2022**, *123* (November), 103472. https://doi.org/10.1016/j.vibspec.2022.103472.

(37) Pullanchery, S.; Yang, T.; Cremer, P. S. Introduction of Positive Charges into Zwitterionic Phospholipid Monolayers Disrupts Water Structure Whereas Negative Charges Enhances It. *J. Phys. Chem. B* **2018**, *122* (51), 12260–12270. https://doi.org/10.1021/acs.jpcb.8b08476.

(38) Yang, X.; Liu, G.; Huo, L.; Dong, H.; Zhong, H. Alkane Solubilization by Surfactants: Aggregate View and Size Analysis Based on Cryo-TEM. *Colloids Surfaces A Physicochem. Eng. Asp.* **2022**, *642* (November 2021), 128589. https://doi.org/10.1016/j.colsurfa.2022.128589.

(39) Tokuoka, Y.; Uchiyama, H.; Abe, M.; Ogino, K. Solubilization of Synthetic Perfumes by Nonionic Surfactants. *J. Colloid Interface Sci.* **1992**, *152* (2), 402–409. https://doi.org/10.1016/0021-9797(92)90042-K.

(40) Al-Sabagh, A. M.; Nasser, N. M.; Migahed, M. A.; Kandil, N. G. Effect of Chemical Structure on the Cloud Point of Some New Non-Ionic Surfactants Based on Bisphenol in Relation to Their Surface Active Properties. *Egypt. J. Pet.* **2011**, *20* (2), 59–66. https://doi.org/10.1016/j.ejpe.2011.06.006.

(41) Weiss, J.; Coupland, J. N.; Brathwaite, D.; McClements, D. J. Influence of Molecular Structure of Hydrocarbon Emulsion Droplets on Their Solubilization in Nonionic Surfactant Micelles. *Colloids Surfaces A Physicochem. Eng. Asp.* **1997**, *121* (1), 53–60. https://doi.org/10.1016/S0927-7757(96)03742-9.
(42) S.Karaborni,'N.M.vanOs,K.Esselink, andP. A. J. H. Molecular Dynamics Simulations of Oil Solubilization in Surfactant Solutions. *Langmuir* **1993**, *9*, 1175–1178.

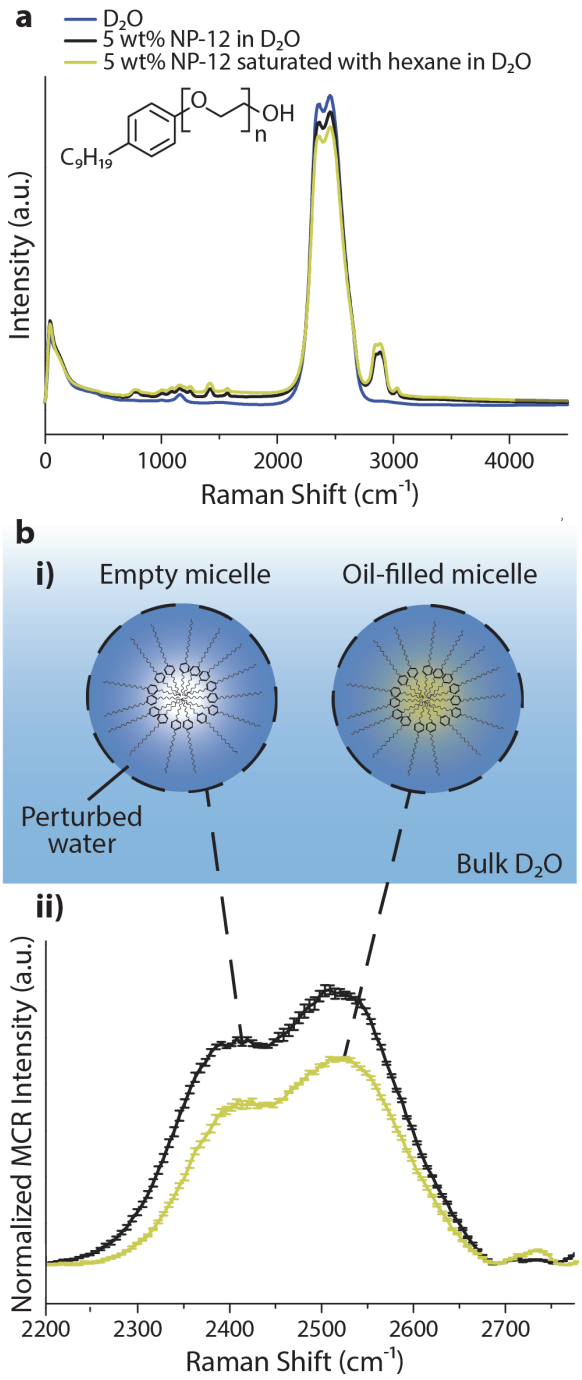

Figure 1: Raman multivariate curve resolution (MCR) provides insight regarding the perturbation of water within and around micelles. **a)** Overlayed Raman spectra of pure D_2O (blue line), 5 wt% Tergitol NP-12 micelles in D_2O (black line), and 5 wt% Tergitol NP-12 micelles saturated with hexane (yellow line). Tergitol NP-12 structure is shown where *n* is an average of 12. **b-i)** Schematic showing a simplified version of a Tergitol NP-12 micelle. The empty (unsaturated) micelle is on the left, where the perturbed water is shown in dark blue inside of the dotted lines, and the oil-filled (saturated micelle) is shown on the right with oil inside of the micelle. **b-ii)** Normalized MCR intensity of 5 wt% Tergitol NP-12 in D_2O (black line) and 5 wt% Tergitol NP-12 micelles saturated with hexane (yellow line) showing that oil saturation of hexane into the micelle decreases the amount of perturbed water in the system (less water inside of dotted lines in schematic). Error bars are the standard deviation of three runs.

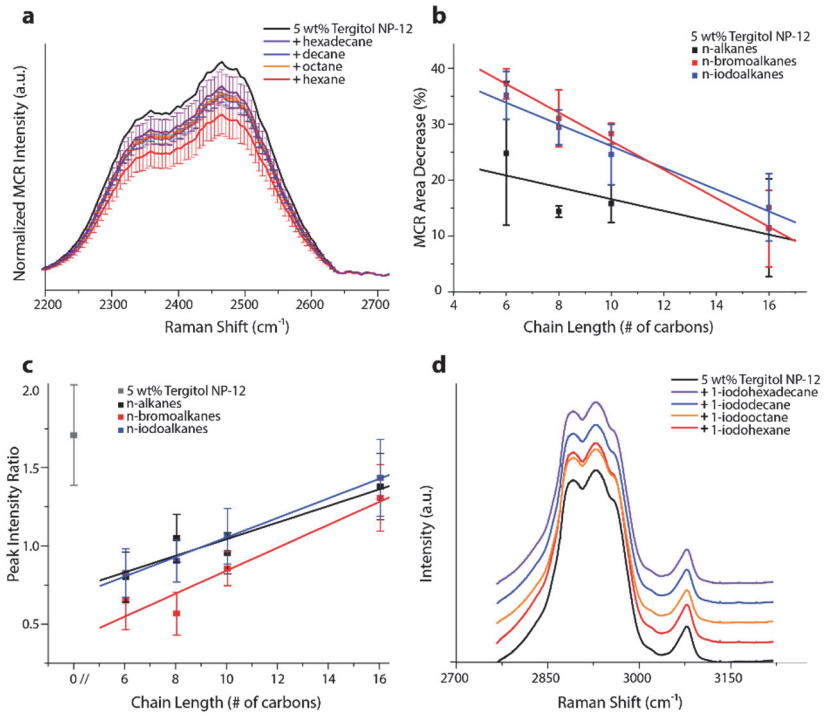

Figure 2: MCR analysis reveals trends in hydrophobic hydration for micelles swollen with oils of varying length and halogenation. a) Representative MCR spectra of 5 wt% Tergitol NP-12 (black) and spectra of the processed average of four independent trials of 5 wt% Tergitol NP-12 saturated with hexadecane (violet), decane (blue), octane (orange), and hexane (red). The data was processed to display the average and standard deviation of the observed OH intensity decrease in the MCR spectra compared to the unsaturated micelle by multiplying the unsaturated micelle spectrum (black) by the average percent decrease of each saturated micelle. The spectra were normalized to the CH region of the spectrum. **b)** MCR area percent decrease of 5 wt% Tergitol NP-12 micelles saturated in n-alkanes (black), n-bromoalkanes (red), and n-iodoalkanes (blue) as a function of carbon chain length. Error bars are standard deviation of 3 trials (9 runs total). **c)** The peak intensity ratio of aromatic OH (2703 cm^{-1}) to free OH (2732 cm^{-1}) of the MCR spectrum of n-alkanes (black), n-bromoalkanes (red), and n-iodoalkanes (blue) as a function of carbon chain length. Error bars are standard deviation of 3 trials (9 runs total). **d)** The CH region (2800-3150 cm^{-1}) of the Tergitol NP-12 micelles as a function of n-iodoalkane chain lengths. Lines on graph have been spaced in order to aid in visualization of peaks.

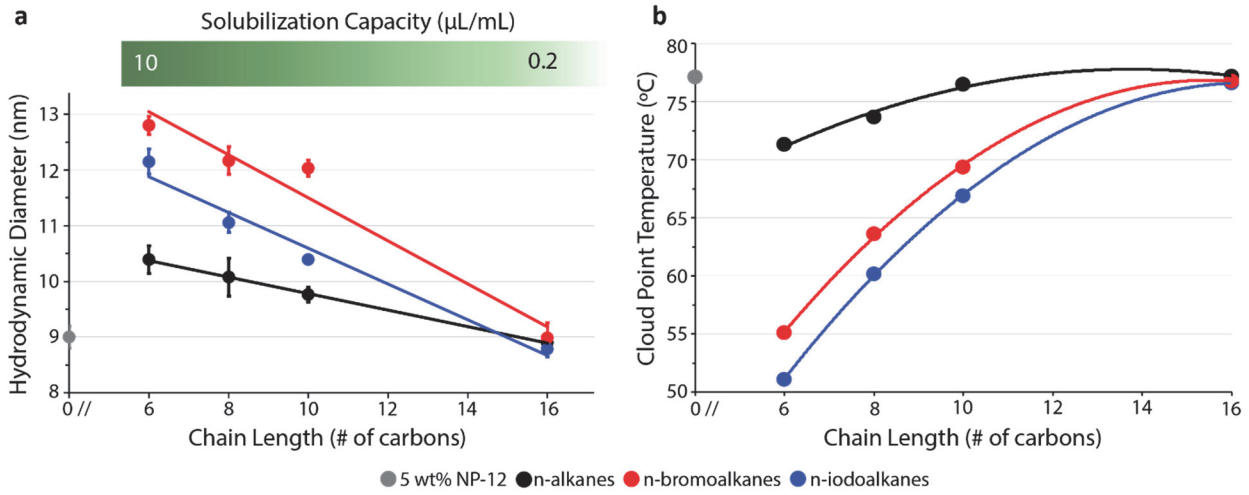

Figure 3: Observed trends in micelle hydrodynamic diameter, solubilization capacity, and cloud point of 5 wt% Tergitol NP-12. a) Graph of hydrodynamic diameter of 5 wt% Tergitol NP-12 micelles versus oil chain length solubilized into the micelle, where the unsaturated empty micelle diameter is shown in light grey, micelles with n-alkanes solubilized shown in black, micelles with n-bromoalkanes solubilized shown in red, and micelles with n-iodoalkanes solubilized shown in blue. Error bars are the standard deviation of three measurements (9 runs total). The approximate range of solubilization capacity is shown above. Refer to **Table S1-S2**. **b)** Graph of cloud point temperature of 5 wt% Tergitol NP-12 micelles versus oil chain length solubilized into the micelle, where the unsaturated empty micelle cloud point is shown in light grey, micelles with n-alkanes solubilized shown in black, micelles with n-bromoalkanes solubilized shown in red, and micelles with n-iodoalkanes solubilized shown in blue. Error bars are plotted but are encompassed in the size of the marker (error 0.1-0.2 °C), error bars are standard deviation of three measurements (9 runs total). Lines on the graph are only meant to guide the eye.

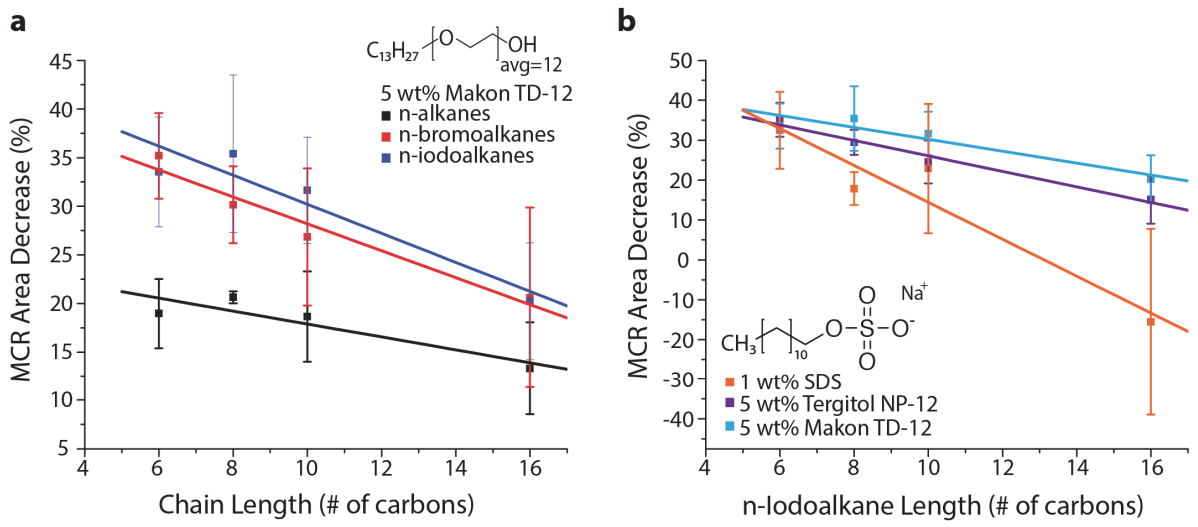

Figure 4: MCR analysis of different surfactants and the impact of oil solubilization on hydrophobic hydration. a) MCR area percent decrease for 5 wt% Makon TD-12 micelles saturated with n-alkanes (black), n-bromoalkanes (red), and n-iodoalkanes (blue) as a function of carbon chain length. Error bars are standard deviation of 3 trials (9 runs total). **b)** MCR area percent decrease of 1 wt% SDS (orange), 5 wt% Tergitol NP-12 (purple), and 5 wt% Makon TD-12 (light blue) as a function of n-iodoalkane length. Error bars are standard deviation of 3 trials (9 runs total).